First-principles prediction of phase-segregating alloy phase diagrams and a rapid design estimate of their transition temperatures

N. A. Zarkevich,* Teck L. Tan, and D. D. Johnson†
Department of Materials Science and Engineering, University of Illinois, Urbana-Champaign, Urbana, Illinois 61801, USA
(Received 19 September 2006; revised manuscript received 22 December 2006; published 21 March 2007)

We calculate the transition temperature versus concentration (T_c vs c) phase diagrams of several phase-segregating alloys [fcc Ca-Sr, Au-Pt, and Rh-(Pd,Cu,Ag,Au)] using a multiscale method combining first-principles calculations and Monte Carlo via the cluster expansion (CE). We study Pd-Rh, with its well-known high-T miscibility gap, to verify the method's reliability. We predict that Ca-Sr segregates at low temperatures. We then show that a rapid estimate of T_c is obtained from enthalpies analytically derived from a CE, and, using thermodynamic integration, we determine under what circumstances this mean-field estimate is accurate compared to Monte Carlo results. Also, we discuss how an electronegativity difference of the alloying elements quickly assess when vibrational entropy effects should be included in the estimate of T_c.

DOI: 10.1103/PhysRevB.75.104203 PACS number(s): 81.30.Bx, 64.70.Kb, 71.55.Ak, 89.20.−a

I. INTRODUCTION

First-principles density-functional theory combined with statistical methods via evolving cluster expansion (CE) techniques is a valuable multiscaling tool[1–9] that can be used to predict alloy thermodynamics.[10–21] Knowledge of the ground states and the temperature (T) versus composition (c) phase diagrams are of crucial importance in materials design. Unfortunately, low-temperature phase transitions are often difficult to observe experimentally due to slow kinetics. Yet, sometimes unexpected phase transitions are responsible for catastrophic failures of aging materials. Thus, multiscale theoretical and computational methods, including rapid estimates of phase stability, are important in materials design and for safety verification.

Here we apply these methods to several face-centered-cubic (fcc) based alloys, focusing mainly on Ca-Sr (prediction) and Pd-Rh (validation), especially to study rapid estimations of T_c. Pd-Rh has a well-known miscibility gap,[22–25] previously studied theoretically,[26–29] hence it is perfect for assessing simple methods for estimating transition temperature T_c. Being both from group 2*A* alkaline earth metals, the more chemically active radioactive Sr isotope has tendency to replace Ca in living organisms. The assessed Ca-Sr phase diagram[25,30] shows a solid-solid phase boundary between disordered high-T body-centered cubic and a low-T fcc solid-solution phases, but no known transitions inside the fcc phase. As each alloy is expected to have segregated and/or ordered states at low temperatures, there must be a T_c phase boundary.

We predict T_c versus c diagrams for Ca-Sr and Pd-Rh by two methods: a rapid estimate by a mean-field solution of the Gibbs equation that is an analytic *a priori* output from the cluster expansion, and Monte Carlo simulation. Using thermodynamic integration, we determine under what circumstances for the derived interactions in these alloys the mean-field solution is accurate. For Pd-Rh, we compare our results to experimental data and show that results from both methods are accurate. We use the methods on (Cu, Ag, Au)-Rh and Au-Pt for trends. We conclude by comparing results to other mean-field estimates and discuss how vibrations will affect our results, including a means to assess *a priori* when vibrational effects are important.

II. METHODS

We combine first-principles density-functional theory (DFT) calculations, which are used to create a reliable database of structural formation enthalpies, with Monte Carlo methods based upon the cluster expansion (CE) methods.[1] We have implemented, and continue to enhance, the computational Thermodynamic Tool-Kit[31] (TTK) for this type of multiscale modeling.

A. Enumeration of alloy configurations

We use the "smallest-first" algorithm[32,33] to generate different fcc alloy configurations (structures) via TTK,[31] and supplement with long-period superstructures.[1] All the structures with different interatomic correlations are uniquely enumerated. Structures with the smaller number of sites (atoms) per primitive cell appear before larger ones. The first structure has one atom per fcc primitive cell, it is A1 $cF4$ (Cu) structure with $Fm\bar{3}m$ space group (No. 225). The second structure with two atoms per primitive cell is $L1_0$ $tP2$ (CuAu) structure with $P4/mmm$ space group (No. 123), with the translation vectors $(-2,0,0)$, $(0,-1,1)$, (0, 1, 1). Within the same number of sites per cell, structures with shorter translation vectors appear first. The third structure has two atoms per primitive cell and the translation vectors $(-2,-1,-1)$, $(0,-1,1)$, $(-1,0,1)$. These vectors are sorted by length (longest first). Fourth and fifth are $oI6$ ($MoPt_2$) structures with three atoms per cell at compositions of 1/3 and 2/3, respectively. Similarly, the first two structures with four atoms per primitive cell are $L1_2$ $cP4$ (Cu_3Au) at compositions of 1/4 and 3/4, which are the 10th and 11th structures.

The "smallest-first" algorithm[32] can be used for enumerating structures on any fixed lattice. Although consideration of only a limited set of the smallest structures bears the risk of missing long-range interactions (or, as we have shown,[1] long-period superstructures), such interactions are not important in the phase-segregating systems considered here. Even in the case of using another set of larger structures, the "smallest-first" algorithm can be used for enumerating and descriptive purposes.

B. DFT calculations

Electronic energies of various atomic structures are calculated via the Vienna *ab initio* Simulation Package (VASP)[34]—a pseudopotential code using projector augmented-wave (PAW) basis sets[35,36] and the generalized-gradient approximation[37] (GGA). We used a plane-wave energy cutoff of 425 eV for Ca-Sr and 400 eV for Pd-Rh, and converged Brillouin zone integration meshes[38,39] with at least 16^3 k points/cell (51 points/Å^{-1} for Ca-Sr and 35 points/Å^{-1} for Pd-Rh). All the structures were relaxed using the conjugate-gradient algorithm within VASP so that pressures were below 10 kBar and atomic forces did not exceed 0.03 eV/Å.

C. Cluster expansion

We find effective interatomic interactions from a set of DFT structural enthalpies using a CE basis.[1] On a fixed lattice having N sites any alloy configuration σ can be represented by a set of occupational variables $\{\xi\}$, with ξ_p being 1 (0) if site p is (not) occupied by solute. We assume that all sites are occupied. An ensemble average occupation probability gives the solute concentration, i.e.,

$$\langle \xi \rangle_\sigma = \frac{1}{N}\sum_p^N \xi_p(\sigma) = c(\sigma). \tag{1}$$

In the disordered phase $\langle \xi_p \rangle = c$ for each site p.

A cluster is a fixed set of lattice sites. All possible clusters of lattice sites $\{p\}_{nfd}$ can be enumerated. Here n is the number of sites within the cluster (e.g., $n=2$ for pairs); f enumerates symmetry-distinctive shapes of the n-site clusters (e.g., $f=1$ for nearest and $f=2$ for next-nearest neighbors); smaller clusters have smaller indices. Index d distinguishes symmetry-equivalent n-body clusters of shape f. Because ξ_p is either 0 or 1 for any given site p of a fixed configuration σ, a product $\Pi_{p_i \subset \{p\}_{nfd}} \xi_{p_i}$ is also either 0 or 1 for a fixed set of sites $\{p\}_{nfd}$ including site p. The n-site correlation function

$$\bar{\Phi}_{nf}(\sigma) = \langle \xi_{p_1} \cdots \xi_{p_n} \rangle_\sigma = \frac{1}{N D_{nf}} \sum_p^N \sum_d^{D_{nf}} \prod_{p_i \subset \{p\}_{nfd}}^n \xi_{p_i}(\sigma) \tag{2}$$

is an ensemble average bounded by $0 \leqslant \bar{\Phi}_{nf} \leqslant 1$. The number of symmetry-equivalent clusters including one particular site p is called "degeneracy" D_{nf}; for example, for fcc lattice $D_{21}=12$ accounts for the number of nearest-neighbor pairs. In the homogeneously disordered state with no short-range order $\langle \Pi \xi_p \rangle = \Pi \langle \xi_p \rangle$ and

$$\bar{\Phi}_{nf}(c) = c^n. \tag{3}$$

In the disordered phase the atomic pair correlations $\bar{\Phi}_{2f}(c)$ describe the atomic short-range order.

Enthalpy of any atomic configuration σ

$$H(\sigma) = \frac{1}{N}\sum_p^N \xi_p \sum_{n,f} \tilde{V}_{nf} \frac{1}{n} \sum_d^{D_{nf}} \prod_{i=2}^n \xi_{p_i} \tag{4}$$

(where $p_i \subset \{p\}_{nfd}$ and $p_i \neq p$) can be written in terms of averaged correlations $\bar{\Phi}_{nf}(\sigma)$ defined by Eq. (2) and weighted effective cluster interactions $V_{nf} \equiv D_{nf}\tilde{V}_{nf}/n$, namely,

$$H(\sigma) = \sum_{n,f} V_{nf} \bar{\Phi}_{nf}(\sigma). \tag{5}$$

Enthalpy of the fully disordered state is

$$H_d(c) = \sum_n c^n \sum_f V_{nf}. \tag{6}$$

Often it is convenient to use formation enthalpy relative to $H(c=0) \equiv H(0) = V_0$ and $H(1) = \Sigma_{nf} V_{nf}$, i.e.,

$$\begin{aligned} \Delta H^F(\sigma) &= H(\sigma) - [(1-c)H(0) + cH(1)] \\ &= \sum_{n \geqslant 2} \sum_f [\bar{\Phi}_{nf}(\sigma) - c] V_{nf}. \end{aligned} \tag{7}$$

We find V_{nf} by fitting a set of $\Delta H^F(\sigma)$ obtained from DFT. Using these interactions, we identify the ground states (here only fcc), calculate the enthalpy of the fully disordered phase versus c, and perform thermodynamic modeling using mean-field theory and Monte Carlo.

In general, the cluster expansion Hamiltonian (4) can be further extended to include effects of vibrations,[14] elasticity,[40–42] magnetism,[43] etc. These additional effects are unimportant in the nonmagnetic, segregating alloys considered here. As we discuss later, vibrational effects are negligible in alloys when the constituting elements have similar electronegativities.[44–47] Anisotropic strain and long-range order effects are irrelevant for disordered phase-segregating alloys considered here, but may play a very important role in other systems.[12,13,40,48]

D. Estimating predictive errors

If V_{nf} are known, enthalpy of any atomic configuration σ with correlations $\bar{\Phi}_{nf}(\sigma)$ can be predicted with the CE (5). Errors associated with CE enthalpies may be evaluated using a standard statistical measure of exclude-m cross-validation (CV) score[49–51]

$$\varepsilon_m^2 = \frac{1}{M}\sum_{i=1}^M \frac{1}{C_{m-1}^{M-1}} \sum_{j=1}^{C_{m-1}^{M-1}} (H^i_{\mathrm{DFT}} - H^i_{\mathrm{CE}(M-m_j)})^2. \tag{8}$$

Here $H^i_{\mathrm{CE}(M-m_j)}$ is *predicted* by a fit to $(M-m)$ DFT enthalpies *excluding* a set m_j of m DFT enthalpies, one of which is H^i_{DFT}. The number of possible sets m_j is given by $C_{m-1}^{M-1} = (M-1)!/[(m-1)!(M-m)!]$.

Thus, ε_0 yields a least-squares fit error, measuring how well the CE reproduces the known *fitted* DFT enthalpies. Error in the predicted unknown values can be estimated by an exclude-m CV score ε_m, if m new values are predicted simultaneously. The exclude-one CV score

$$\varepsilon_1 = \left[\frac{1}{M}\sum_{i=1}^M (H^i_{\mathrm{DFT}} - H^i_{\mathrm{CE}(M-1_i)})^2 \right]^{1/2} \tag{9}$$

estimates an uncertainty in predicting one excluded or unknown structural formation enthalpy ΔH^F. Both too few (underfitting) or too many (overfitting) parameters give poor

prediction, so ε_1 has a minimum.[1,52] Previously it was suggested to select the best CE by minimizing the predictive error estimated by ε_1.[1,52,53] However, for correlated data ε_1 is not always a good estimate of the predictive error. In general, we can put an error bar on ε_m by $\varepsilon_{m-1} \leqslant \varepsilon_m \leqslant \varepsilon_{m+1}$. In particular, if ε_2 is infinite, ε_1 has an infinite upper error bar. Only if ε_2 is finite can we use ε_1 to estimate the CE predictive error for a well-defined compact cluster basis.[1] Total error in predicted thermodynamics arises from cumulative errors in the DFT, CE, and Monte Carlo statistics.[2]

E. Rapid estimate of T_c

Because change of Gibbs free energy $\Delta G(T)=\Delta H(T)-T\Delta S(T)$ is zero at a first-order transition at T_c, where ΔH and ΔS are changes in enthalpy and entropy between the two coexisting phases at T_c,

$$T_c(c) = \frac{\Delta H(T_c,c)}{\Delta S(T_c,c)}, \tag{10}$$

Equation (10) is exact; however, the ratio is difficult to find directly. For given interactions V_{nf}, estimates of T_c can be made quickly using mean-field approximation, or a relatively accurate value can be calculated by Monte Carlo methods.

1. Mean-field "T_0" estimate

T_c can be quickly estimated by assuming that $\Delta H(T_c)$ in Eq. (10) is proportional to the difference between $T=\infty$ fully disordered and $T=0$ fully ordered states, i.e., $\Delta H_{d-o}=H(T=\infty)-H(T=0)$, and similarly for the entropy. Then

$$T_c(c) \approx \frac{\Delta H_{d-o}(c)}{\Delta S_{d-o}(c)} \equiv T_c^{\text{est}}(c) \tag{11}$$

is a standard mean-field approximation, often called the "T_0" line.[3,27,54] Entropy of a single fully ordered or phase-segregated state is zero, while that of the fully disordered state is given by only the point entropy, i.e.,

$$S_d(c) = -k_B[c \ln c + (1-c)\ln(1-c)]. \tag{12}$$

The difference in enthalpy (11) can be calculated trivially within the cluster expansion using Eqs. (5) and (6). For phase segregation, as is the case for Ca-Sr and Pd-Rh,

$$\Delta H_{d-o}(c) = \Delta H_d^F(c) = \sum_{n\geqslant 2} (c^n - c) \sum_f V_{nf}. \tag{13}$$

Although $\Delta H(T_c)$ in Eq. (10) is typically orders of magnitude smaller than ΔH_{d-o} in Eq. (11), and the same is also true for ΔS, the mean-field estimate is accurate if and only if the ratio $\Delta H/\Delta S$ in Eqs. (10) and (11) is approximately the same, which should be the case for a large class of systems identified by the underlying interactions.

We suggest that the approximation (11)–(13) is expected to be accurate for alloys with competing (pair and multibody) interactions, which lower the enthalpy and entropy differences due to atomic correlations (clustering here) such that the ratio in Eq. (10) remains approximately equal to that in Eq. (11), as we show in the results. The rapid estimate $T_c^{\text{est}}(c)$ from Eq. (11) provides an accurate $T_c(c)$ for Pd-Rh and Ca-Sr at all c except those near $c=0$ and $c=1$, where both ΔH and ΔS approach zero.

2. Mean-field "Bethe" estimate

T_c can be also quickly estimated using another first-order mean-field theory by Bethe for the zero-field Ising ferromagnet (equivalent to a clustering 50% binary).[55–57] Bethe improved the Weiss molecular-field theory by including the short-range correlations in order to enforce agreement between the average magnetization on the central site and nearest neighbors. The well-known solution in terms of the nearest-neighbor pair $\tilde{V}_{21}$ in Eq. (4) is

$$T_c^{\text{Bethe}} = \frac{\tilde{V}_{21}}{2k_B}\left[\ln\left(\frac{q}{q-2}\right)\right]^{-1}, \tag{14}$$

where q is the coordination number of the Bravais lattice (e.g., 12 for fcc). In the limit where mean-field theory is exact (i.e., $q\to\infty$) the Weiss result of $q\tilde{V}_{21}/4k_B$ is recovered, whereas the fcc nearest-neighbor-only T_c^{Bethe} result is lower by a factor of 1.0939. More notably, for the Ising ferromagnet, the Bethe approximation predicts the correct behavior of T_c in d dimensions; for example, in $2d$ with $q=2$, T_c^{Bethe} is zero, the correct answer.[57]

While Bethe derived the theory for a nearest-neighbor pair interaction, it is straightforward to extend his derivation (in the same approximations) to pair interactions of arbitrary range, which we write for an alloy using Eq. (7) as

$$T_c^{\text{Bethe2}} = \frac{2\Delta H_d^F(c)}{k_B}\left[\frac{q_{\text{eff}}}{2}\ln\left(\frac{q_{\text{eff}}}{q_{\text{eff}}-2}\right)\right]^{-1}, \tag{15}$$

where the effective coordination number is

$$q_{\text{eff}} = \sum_{f=1}^{N} \frac{\tilde{V}_{2f}}{\tilde{V}_{21}} D_{2f}. \tag{16}$$

For interactions $\tilde{V}_{2f}$ held constant and equal to $\tilde{V}_{21}$, independent of range, for all shells of neighbors, the Weiss result of $q\tilde{V}_{21}/4k_B$ is recovered. Note that for a phase-segregating alloy, T_c is estimated as $2\Delta H_{d-o}(c)/k_B$ for long-range, clustering-only pair interactions.

Extending the Bethe approximation to ordering (antiferromagnetic) interactions (and its longer-range, competing interaction, variant) is tenuous because it is sensitive to the lattice topology, even for the ferromagnetic case.[58,59] The same is true for the extension to the general multibody interaction case. The Bethe approximation is exact, however, in the limit that $\tilde{V}_{2f}$ are only clustering and long ranged. More importantly, for clustering-only $\tilde{V}_{2f}$ (independent of range), T_c^{Bethe2} is independent of entropy change, in contrast to $T_c^{\text{est}}(c)$. Hence, alloys cannot be described, generally, by Bethe or Weiss type theories if they have competing clustering- and ordering-type interactions. Therefore, only at the end will we contrast the results of $T_c^{\text{Bethe2}}(c)$ with $T_c^{\text{est}}(c)$ and $T_c^{\text{MC}}(c)$.

F. Monte Carlo determination of T_c

We also find an accurate T_c by locating maxima in specific heat, using $\tilde{V}_{nf}$ within the lattice Monte Carlo program with Metropolis algorithm[60] as implemented within TTK.[31] We used from 16^3 (or 4096) to 24^3 (or 13 824) atoms within the periodic simulation box. We performed grand-canonical simulations with either fixed chemical potential or fixed temperature, as well as canonical (fixed-composition) simulations with 200-800 equilibration steps and 4000-16000 sampling steps. To perform any noted finite-size scaling, we included up to 32^3 simulation box (32 768 atoms).

G. Thermodynamic integration

In Sec. III D we will investigate the difference in enthalpies and entropies between the two phases versus T and c. To do this we find the enthalpies $\langle H\rangle$ and specific heats $C_v \sim \langle H\rangle^2 - \langle H^2\rangle$ using thermodynamic averages within canonical Monte Carlo. Entropies $S(T,c)$ are then found by thermodynamic integration, i.e.,

$$S(T_+ > T_c) = S_d - \int_{T_+}^{\infty} dT \frac{C_v(T)}{T},$$

$$S(T_- < T_c) = S_o + \int_{0}^{T_-} dT \frac{C_v(T)}{T}, \tag{17}$$

where $S_o = 0$ and S_d in Eq. (12) are known. Near T_c we use a temperature step of approximately 0.01 T_c, while at higher temperatures a significantly coarser temperature integration step can be used.

III. RESULTS

A. Structural formation enthalpies

First-principles calculated formation enthalpies ΔH^F of various fcc Ca-Sr and Pd-Rh structures are given in Fig. 1, where all ΔH^F are positive. Hence we expect both alloys to segregate at low enough temperatures [order of magnitude is roughly $k_B T_c(c) \sim \Delta H_d^F(c)$]. The internal atomic relaxations in all these structures are relatively small compared to interatomic distances, so an effective lattice for both Ca-Sr and Pd-Rh at low temperatures is fcc only (in contrast, for example, to Ca-Ag or Al-Ag).[12,13] Next, there is a small asymmetry of structural enthalpies versus composition; namely, formation enthalpies of similar binary structures (e.g., $L1_2$ or DO_{22} at 25 and 75%) are not the same at c and $(1-c)$, indicating presence of multibody interactions beyond pairs.

Many alloy phase diagrams are known from a combination of experimental data and thermodynamic modeling; hence, the boundaries are estimates, as in the case of Au-Pt, which exhibits an asymmetric miscibility gap with a maximum at 61% Pt.[25] We will focus primarily on Pd-Rh (known) and Ca-Sr (new prediction). However, as found in the Appendix in Fig. 5, Au-Pt exhibits a highly asymmetric formation enthalpies of similar structures, indicating important multibody interactions, and yielding a $\Delta H_d^F(c)$ with a maximum roughly at 62%Pt, in agreement with asymmetry in experiment. Interestingly, in highly cold-work Au-Pt, metastable Au_3Pt has been found, which corresponds to low-energy structures we find at 25 and 33% Pt, see the Appendix for more discussion. We also show similar results for Rh-(Cu,Ag,Au) alloys in the Appendix (see Fig. 5) to provide a trend in segregation going down a column in the Periodic Table. However, the stability of the liquid phase is critical for the Rh-(Ag,Au) systems, and its thermodynamic influence is also very important for the concentrated Rh-Cu and Pt-Au, where $T_c \sim T_{\text{melt}}$, as discussed in Sec. IV B.

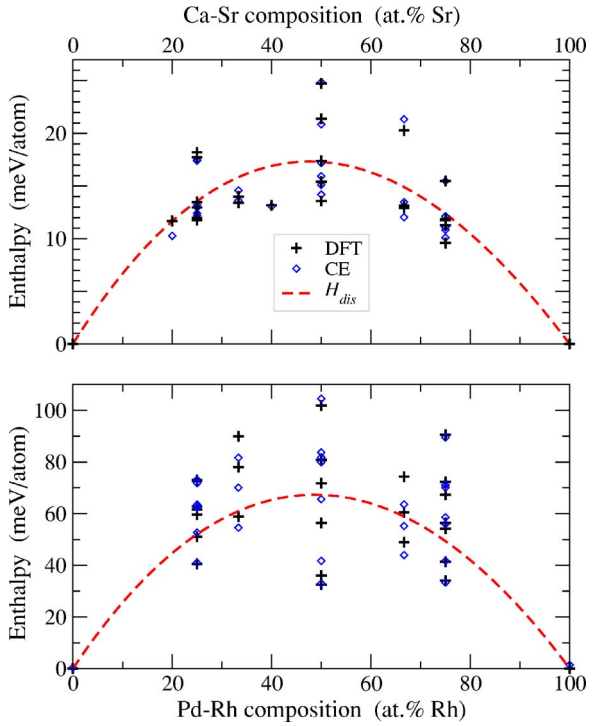

FIG. 1. (Color online) Formation enthalpies of the fcc Ca-Sr (upper) and Pd-Rh (lower) structures from DFT (crosses) and CE (diamonds), with enthalpy of the fully disordered phase (6) included (dashed lines).

B. Interatomic interactions

We used DFT structural enthalpies to find cluster interactions (Table I) within the CE basis.[1] We found several sets of cluster interactions with low fit and predictive errors, all approximately equal; using those equally good sets in Monte Carlo lead to similar results. For Ca-Sr, the set including eight pair and three triplet interactions reproduces the DFT enthalpies well (see Table II), with the exclude-0 (i.e., least-squares fit error), exclude-1 and exclude-2 cross-validation scores ε_0, ε_1, and ε_2 of 0.57, 1.3, and 1.4 meV/atom, respectively. Similarly, we list the Pd-Rh interactions in Tables I and enthalpies in Table II), where the cross-validation errors ε_0, ε_1, and ε_2 are 4.3, 7.5, and 7.7 meV/atom, respectively. While the absolute values of the errors ε_m are several times larger for Pd-Rh, so too are T_c (see Fig. 2), hence, relative CE errors are similar for these two systems. In Table I we see that both systems have pair interactions that drive local clus-

TABLE I. Interactions V_{nf} (5) and $\tilde{V}_{nf}$ (4) in meV with their degeneracies D_{nf} for four alloys.

		Ca-Sr		Pd-Rh		Cu-Rh		Au-Pt	
f	D_{2f}	V_{2f}	$\tilde{V}_{2f}$	V_{2f}	$\tilde{V}_{2f}$	V_{2f}	$\tilde{V}_{2f}$	V_{2f}	$\tilde{V}_{2f}$
1	12	−14.3	−2.39	−330.8	−55.13	229.2	38.19	160.6	26.77
2	6	−21.0	−7.00	−3.8	−1.27	54.5	18.18	55.3	18.42
3	24	−28.4	−2.37	−9.3	−0.77	140.6	11.72	97.6	8.13
4	12	9.1	1.52	5.3	0.88	−29.5	−4.91	9.4	1.56
5	24	−24.7	−2.06			−26.6	−2.21	−24.1	−2.00
6	8	−7.3	−1.83			44.7	11.18	9.5	2.39
7	48	6.4	0.27			−82.7	−3.45	−26.0	−1.08
8	6	−5.2	−1.72					−12.0	−4.00
f	D_{3f}	V_{3f}	$\tilde{V}_{3f}$	V_{3f}	$\tilde{V}_{3f}$	V_{3f}	$\tilde{V}_{3f}$	V_{3f}	$\tilde{V}_{3f}$
1	24	−9.3	−1.16	20.6	2.57	−311.7	−38.96	−424.9	−53.11
2	36	5.3	0.44	5.6	0.47	−67.4	−5.62	−33.2	−2.77
3	72	15.3	0.64	−40.3	−1.68	−493.1	−20.55	−169.4	−7.06
4	18			85.8	14.31	158.5	26.42	−72.7	−12.12
5	72			85.8	14.31	158.5	26.42	−41.9	−1.75
f	D_{4f}	V_{4f}	$\tilde{V}_{4f}$	V_{4f}	$\tilde{V}_{4f}$	V_{4f}	$\tilde{V}_{4f}$	V_{4f}	$\tilde{V}_{4f}$
1	8			−21.8	−10.9	83.4	41.69	10.1	5.07
2	48					4.3	0.36	455.2	37.94
3	48					212.9	17.74	253.0	21.08
f	D_{5f}	V_{5f}	$\tilde{V}_{5f}$	V_{5f}	$\tilde{V}_{5f}$	V_{5f}	$\tilde{V}_{5f}$	V_{5f}	$\tilde{V}_{5f}$
1	30							−186.5	−31.09
2	120							−133.2	−5.55

tering (negative sign) competing with triplet interactions that drive local ordering.

C. Phase diagrams

The calculated fcc phase diagrams are shown in Fig. 2. The Ca-Sr alloy segregates at low temperatures into Ca and Sr, whereas the Pd-Rh alloy has nearly five times larger formation enthalpy (see Fig. 1) and segregates at about five times higher temperature (Fig. 2) due to the stronger two-body interactions, see Table I. Due to three-body interactions, the phase boundary is slightly asymmetric versus c for both Ca-Sr and Pd-Rh, as expected from the small asymmetry of formation enthalpies.

Figure 2 shows phase boundaries $T_c(c)$ calculated by the Monte Carlo and the rapid estimate (11)–(13). One can see that approximation (11) provides an accurate estimate for Monte Carlo T_c for Pd-Rh and Ca-Sr at all c except those near $c=0$ and $c=1$ where both ΔH and ΔS approach zero. For Pd-Rh both the $T_c(c)$ from Monte Carlo and Eq. (11) agree very well with experiment.[23–25]

The total error in calculated transition temperatures includes DFT, predictive, and statistical errors, with the predictive one being the largest.[2] Each error can be estimated. As explained in Sec. II D, the predictive error in CE structural enthalpies can be estimated by the cross-validation score ε_1, but only if ε_2 is finite. We estimate an error bar on T_c (ε_1 plus 1 meV DFT and statistical errors) to be 30 K (2.5 meV) for Ca-Sr and 100 K (8.5 meV) for Pd-Rh. In Fig. 2 one can see that both the rapid estimate and Monte Carlo results for Pd-Rh agree with experiment[24] within the error bar.

D. Enthalpy and entropy changes vs T and c

As noted earlier, the exact T_c can be found from Eq. (10) via the ratio of $\Delta H(T_c)$ and $\Delta S(T_c)$, which are the enthalpy and entropy differences, respectively, between two phases coexisting at T_c. With $0<\kappa<1$, we define

$$\Delta H(\kappa) \equiv H(T_c/\kappa) - H(\kappa T_c), \tag{18}$$

and similarly for the entropy. The limits of Eq. (18) are

$$\lim_{\kappa\to 1}^{\kappa\to 0} \Delta H(\kappa) = \begin{cases} H_d(\infty) - H_o(0) \equiv \Delta H_{d-o}, \\ H(T_c^+) - H(T_c^-) = \Delta H(T_c), \end{cases} \tag{19}$$

where the $\kappa\to 0$ limit is analytically obtained from the CE and $\kappa\to 1$ limit is from careful Monte Carlo calculations. The calculated $\Delta H(\kappa)$, $\Delta S(\kappa)$, and their ratio for $Pd_{75}Rh_{25}$ are shown in Fig. 3. Clearly, the ratio $\Delta H(\kappa)/\Delta S(\kappa)$ does not strongly depend on κ. Thus,

$$T_c = \frac{\Delta H(\kappa=1)}{\Delta S(\kappa=1)} \approx \frac{\Delta H(\kappa=0)}{\Delta S(\kappa=0)} \equiv \frac{\Delta H_{d-o}}{\Delta S_{d-o}}. \tag{20}$$

TABLE II. DFT and CE enthalpies (meV/atom) and their difference for the fcc Ca-Sr and Pd-Rh structures with concentration c relative to the elements. CV errors for Ca-Sr are ε_0=0.57, ε_1=1.33, and ε_2=1.42 meV/atom. CV errors for Pd-Rh are ε_0=4.3, ε_1=7.5, and ε_2=7.7 meV/atom.

		Ca-Sr			Pd-Rh		
Structure	c	H_{DFT}	H_{CE}	Error	H_{DFT}	H_{CE}	Error
Ca	0	0.0	0.7	0.74			
Sr	1	0.0	−0.1	−0.07			
Pd	0				0.0	0.4	0.38
Rh	1				0.0	1.4	1.42
2 $L1_0$	1/2	15.4	15.9	0.50	101.9	104.5	2.68
3	1/2	24.7	24.9	0.12	80.7	81.8	1.10
4	1/3	13.4	13.6	0.21	74.3	63.6	−10.74
5	2/3	13.1	13.5	0.35	89.9	81.7	−8.28
6	1/3	14.0	14.6	0.58	60.5	55.2	−5.29
7	2/3	12.9	12.0	−0.88	78.0	70.1	−7.89
8	2/3				49.0	44.0	−5.01
9	2/3	20.3	21.4	1.06	58.9	54.6	−4.33
10 $L1_2$	1/4	13.0	13.0	0.02	90.5	89.5	−0.99
11 $L1_2$	3/4	11.3	11.1	−0.19	73.1	73.2	0.10
12 DO_{22}	1/4	13.5	13.2	−0.29	67.3	70.0	2.73
13	1/2	17.4	17.2	−0.21	80.9	83.7	2.79
14 DO_{22}	3/4	11.9	12.1	0.28	72.7	71.8	−0.85
15	3/4				56.5	58.6	2.14
16	1/2				71.8	79.9	8.14
17	1/4				61.6	62.7	1.06
18	1/4	18.2	17.5	−0.70	72.3	71.0	−1.24
19	3/4	15.5	15.5	0.00	62.9	63.5	0.66
20	1/4	11.7	12.4	0.68	54.2	56.0	1.77
21	1/2	15.4	15.1	−0.30	56.5	65.6	9.12
22	3/4	11.8	10.8	−0.92	59.7	62.3	2.63
23	1/4	12.0	12.2	0.24	41.4	41.8	0.37
24	1/2	13.6	14.2	0.62	36.1	41.7	5.67
25	3/4	9.6	10.1	0.51	51.0	52.7	1.62
26	1/4	17.7	17.4	−0.33	34.1	33.3	−0.78
27	1/2	21.4	20.9	−0.52	32.5	33.0	0.52
28	1/4				40.5	41.0	0.50
45	1/5	11.7	10.3	−1.41			
46	2/5	13.2	13.1	−0.10			

However, T_c^{est} from (11) is invalid near c=0 and 1 due to $\Delta H(c,T)$ and $\Delta S(c,T)$ approaching zero with different asymptotics. In Figs. 3 and 4 $\langle H\rangle$ and C_v were calculated as given in Sec. II G. Figure 4 shows the calculated ratio $\Delta H(\kappa,c)/\Delta S(\kappa,c)$ at fixed κ of 0.93 versus c. One can see that the relative differences $\Delta H(\kappa)/H_{d-o}$ and $\Delta S(\kappa)/S_{d-o}$ at most compositions are the same. Thus the ratio of $[\Delta H(\kappa)/\Delta S(\kappa)]$ to $[H_{d-o}/S_{d-o}]$ is roughly 1, except near c=0 and 1 for reasons stated above.

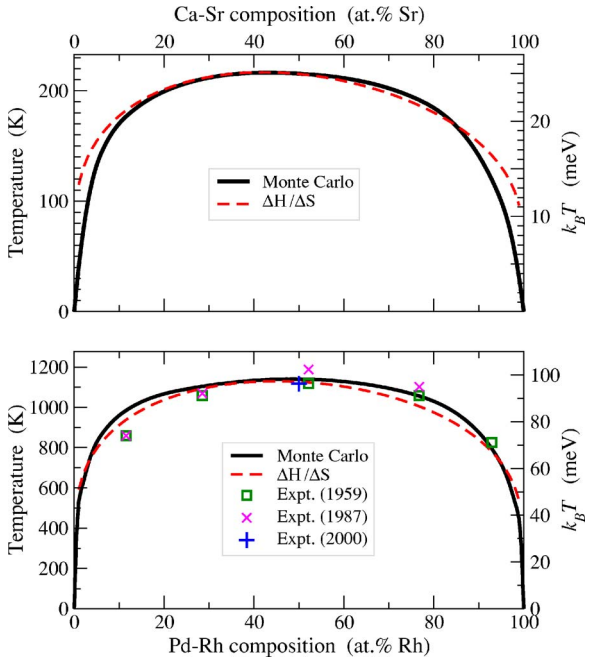

FIG. 2. (Color online) Ca-Sr and Pd-Rh T-c phase diagrams. Miscibility gap from Monte Carlo (solid line) and Eq. (11) estimate (dashed line), compared to experimental data (Refs. 23–25).

Together the results from Figs. 2–4 show that Eq. (11) provides reliable estimates for the segregating alloys, if, in addition, the difference in electronegativity of the constituting elements is small (which implies vibrations are not important, as discussed below). Segregation can be ascertained in a cluster expansion from disordered enthalpy before any Monte Carlo simulations are performed.

In summary, in alloys where vibrational effects are unimportant we have shown that an analytic, mean-field estimate

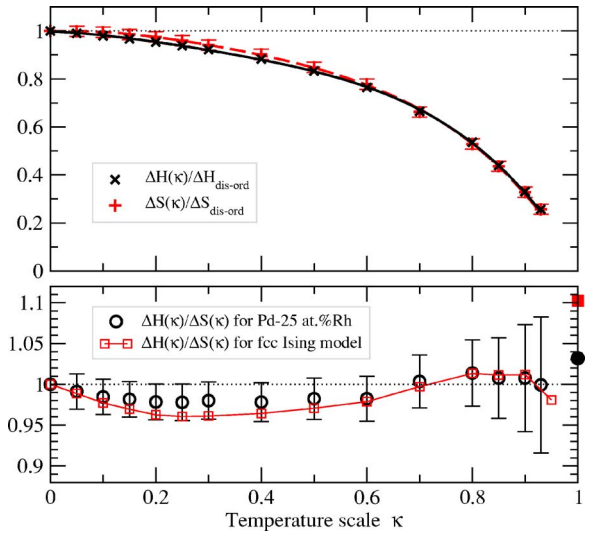

FIG. 3. (Color online) For $Pd_{75}Rh_{25}$ using Eq. (18), enthalpy $\Delta H(\kappa)/\Delta H_{d-o}$, entropy $\Delta S(\kappa)/\Delta S_{d-o}$, and their ratio (circles), along with same results for the fcc nearest-neighbor pair Ising model (squares). Filled symbols at κ=1 are Monte Carlo T_c relative to $(\Delta H_{d-o}/\Delta S_{d-o})$. Results are obtained using a fixed 24^3-atom periodic box. Error bars are given and lines are a guide to the eye.

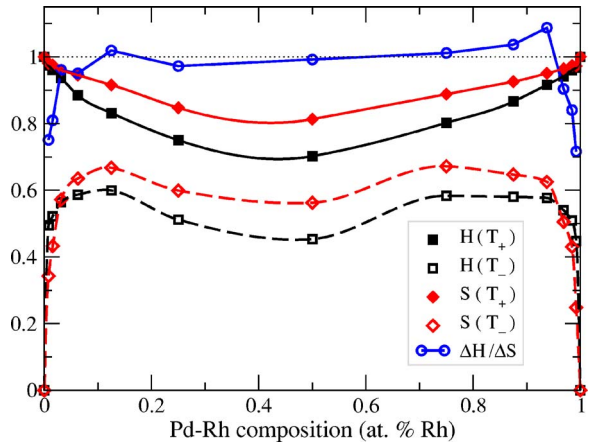

FIG. 4. (Color online) Composition dependence of $H(T_c^+,c)=H(T_c/\kappa,c)$ and $H(T_c^-,c)=H(\kappa T_c,c)$ relative to ΔH_{d-o}, $S(T_c^+,c)$ and $S(T_c^-,c)$ relative to ΔS_{d-o}, and the ratio $\Delta H(\kappa,c)/\Delta S(\kappa,c)$ relative to $\Delta H_{d-o}(c)/\Delta S_{d-o}(c)$ for $\kappa=0.93$. Lines are a guide to the eye.

from the cluster expansion given by T_c^{est} in Eq. (11) is accurate and involves no simulation—useful for rapid design estimates. Via Monte Carlo based thermodynamic integration, we illustrated the validity of this estimate versus composition and temperature scale. Below, we contrast this with the Bethe (pair-only) mean-field theory that becomes exact for infinite-ranged pair interactions, and show that without competing interactions the T_c^{est} is inaccurate. We then discuss the effects of vibration on the prediction of T_c.

IV. DISCUSSION

A. Comparison to previous results

Unlike fcc Ca-Sr, Pd-Rh was previously studied both experimentally[22–24] and theoretically.[26–28] Disordered fcc Pd-Rh has been studied via first-principles multiple-scattering theory combined with the coherent-potential approximation (KKR-CPA) for direct calculation of formation enthalpies of the homogeneously disordered state.[27] Even though obtained within the atomic-sphere approximation to the potentials, the previous KKR-CPA enthalpies[27] agree well with our present full-potential results. Also, the KKR-CPA enthalpies were used to find the phase boundary via approximation (11), also in reasonable agreement with experiment.[27]

Pd-Rh was also studied by a CE with interactions fitted to the tight-binding linear muffin-tin orbital results.[28] The difference between the present structural formation enthalpies and the former[28] ones are presumably due to a more approximate electronic-structure method used. The previous phase diagram[28] calculated by combining the CE with the cluster variation method using the tetrahedron-octahedron approximation found fair agreement with experiment; larger deviation from experiment are presumably due to the use of less accurate enthalpies.

Au-Rh was studied experimentally[61–64] and theoretically,[65] where it was noted that Au-Rh has no stable compounds, but no phase diagram was calculated. The calculated formation enthalpy[65] of the lowest-energy $AuRh_3$ is 91 meV/atom, which compares well to our 88 meV/atom for the same structure (same as structure 23 noted in Sec. II A). Au-Pt was studied in Refs. 64 and 66–69, and Ag-Rh was addressed in Refs. 70–73. The previously calculated lowest formation enthalpies[65] of Au_2Pt (9 meV/atom) and $AgRh_3$ (116 meV/atom) agree with our results of 16 and 114 meV/atom, respectively, if it is noted that we used higher plane-wave energy cutoff and four times denser k-point mesh (k-point convergence is not monotonic). In general, CE can be used to search for new ground states in ordering alloys, and to confirm their absence in phase-segregating systems.

B. Influence of other phases

As noted earlier, liquid phase is important in the (Cu,Ag,Au)-Rh and Au-Pt systems, hence, without addressing at least the density (i.e., volume) changes of the liquid phase and its reduction in segregation energetics, we cannot make a direct comparison to experiment. In general, all possible phases, structures, and states s contribute to the statistical sum $\Sigma_s e^{-E_s/k_BT}$, but contributions of higher-energy structures are exponentially suppressed. If all low-energy structures belong to one and the same lattice, and contributions from all other high-energy phases are negligibly small, then the fixed-lattice cluster expansion works well and provides high-accuracy predictions, as is the case for Ca-Sr and Pd-Rh. However, this is not always the case. For example, when a (predicted) solid-solid transition temperature is comparable to (or exceeds) a melting temperature, influence of a liquid phase is significant. The CE takes into account only one crystalline phase, and can provide inaccurate predictions if contributions from other phases (such as the liquid phase) are also important.

To illustrate this, we consider Rh-(Cu,Ag,Au) and Au-Pt alloys, see Fig. 5 and Table V. In Cu-Rh and Au-Pt, T_c^{expt} and $T_{\text{melt}}^{\text{expt}}$ are very close (within 20%), while in Ag-Rh and Au-Rh the predicted T_c exceeds $T_{\text{melt}}^{\text{expt}}$. Note, that if only two phases (such as solid-solution and liquid) contribute significantly, and only one of them is taken into account by a CE (i.e., the fcc-based solid solution here), then the prediction is usually roughly within a factor of 2 from the correct result. Although in such systems the CE-based quick estimates and Monte Carlo results are still in some agreement with each other, the CE itself here does not account properly for the liquid thermodynamic contributions. In Ca-Sr and Pd-Rh only one fcc crystalline phase is important at relevant temperatures, hence $T_c \ll T_{\text{melt}}$, the CE works, $T_c^{\text{est}} \approx T_c^{\text{MC}}$, and for Pd-Rh both agree with experiment. In Cu-rich Cu-Rh, $T_c \ll T_{\text{melt}}$ and the CE should be correct, if vibrational contributions are also included, see below.

C. Comparison to the Bethe theory

Having shown that the rapid estimate in Eq. (11) works well for the Ca-Sr and Pd-Rh systems, the Bethe (pair-only) approximation could also be used to estimate T_c quickly, but not reliably. Also, generally, due to topological frustration, the Bethe approximation does very poorly on fcc-based al-

TABLE III. Ratios of T_c to T_c^{Bethe} from Eq. (15) and T_c^{est} from Eq. (11) for different ranges of interactions for 50% composition. We used $\tilde{V}_{2f}$ interactions from Pd-Rh in Table I.

No. of V_{2f}	T_c/T_c^{Bethe}	T_c/T_c^{est}
1	0.886	1.12
4	0.889	1.13
∞	1.00	1.39

loys with antiferromagnetic (ordering) interactions.[58,74] Table III compares estimate T_c^{est} from Eq. (11) and T_c^{Bethe2} from Eq. (15). The ratios of T_c (obtained from Monte Carlo with careful finite-size scaling analysis) to each of the estimates is calculated for three different sets of pair interactions. For the first two sets we used $\tilde{V}_{2f}$ with the number of neighbor shells N taken as 1 and 4, respectively, from Pd-Rh in Table I and q_{eff} is calculated from Eq. (16). The third case takes the first nearest-neighbor value for Pd-Rh in Table I for all $\tilde{V}_{2f}$, i.e., −55.13 meV (constant) and negative (clustering), with $N \rightarrow \infty$, which is calculated analytically.

Table III shows that the Bethe approximation improves marginally when a few pairs beyond the nearest-neighbor are added. However, in the third case, as N becomes infinite with V_{2f} being constant and negative, where mean-field theory is exact,[75] T_c/T_c^{Bethe} is indeed 1. Hence, the Bethe approximation improves as more pair interactions favoring phase segregation are added.

In contrast, T_c^{est} becomes increasingly worse compared to T_c as more pairs are added. For the third case, where the Bethe approximation is exact, T_c^{est} has a significant error of −28%. In addition, we note that T_c^{est} produces an error of −11% when multibody interactions are just ignored in the CE of Pd-Rh given in Table I. Also, we note that a similar proportional change of the entropy and enthalpy versus temperature is found for a pair-only model (we focus on the Ising model), see Fig. 3. However, as is clear in Fig. 3, the Monte Carlo T_c is 11% larger than the T_c^{est}, in contrast to a multibody case. Taking into account the finite-size scaling, the original CE in Table I gives T_c/T_c^{est} of 1.06 (1.03 for a fixed-size 24^3-atom box, see Fig. 3), suggesting that the presence of the competing multibody interactions is needed for estimate (11) to be reliable. Last, we find that T_c^{est} works well for certain classes of ordering systems too. However, this is beyond the scope of this paper, and will be discussed elsewhere.

D. Effects of vibrational entropy changes on T_c

Up to this point our results have focused on how well T_c^{est} reproduced the time-consuming Monte Carlo results for virtually no cost, as it is obtained directly from the cluster expansion analytically, for the cases where no vibrational effects are included. Vibrational effects add a higher level of complexity and difficulty, as they are as time-consuming computationally as a cluster expansion. It can be shown (e.g., see Ref. 76 or 8) that T_c is altered by changes in harmonic vibrational entropy $\Delta S_{\text{vibr}}^{\alpha\rightarrow\beta}$ from the α-β phase transition

TABLE IV. Elemental configurations of valence electrons, atomic numbers Z, electronegativities χ, fcc lattice constants a (Å), and bulk moduli B (MPa) for the relevant alloys (Ref. 84).

Electrons	Z		χ	a	B
$5s^2$	38	Sr	0.95	6.08	0.118
$4s^2$	20	Ca	1.00	5.58	0.115
$3d^34s^2$	23	V	1.63	3.03	1.65
$3d^{10}4s^1$	29	Cu	1.90	3.62	1.335
$3d^84s^2$	28	Ni	1.91	3.53	1.90
$4d^{10}5s^1$	47	Ag	1.93	4.09	0.981
$4d^{10}5s^0$	46	Pd	2.20	3.89	1.844
$5d^{10}6s^0$	78	Pt	2.20	3.92	2.838
$4d^85s^1$	45	Rh	2.28	3.80	2.758
$5d^{10}6s^1$	79	Au	2.40	4.08	1.766

from solely configurational contributions $T_{c,\text{conf}}^{\alpha\rightarrow\beta}$ in Eq. (10), and can be accounted for in the analysis of T_c^{est} in Eq. (11), as

$$T_c^{\alpha\rightarrow\beta} \approx T_{c,\text{conf}}^{\alpha\rightarrow\beta}\left(1+\frac{\Delta S_{\text{vibr}}^{\alpha\rightarrow\beta}}{\Delta S_{\text{conf}}^{\alpha\rightarrow\beta}}\right)^{-1}. \tag{21}$$

For phase-segregating systems studied here $\Delta S_{\text{conf}}^{\alpha\rightarrow\beta}$ is ΔS_{d-o} from Eq. (12). The more correct and computationally expensive quasiharmonic corrections to vibrational entropy, i.e., $\Delta_{\text{QH}}=(\Delta S_{\text{QHvibr}}-\Delta S_{\text{vibr}})/2$, account for the effects of thermal expansion, which typically increase the lattice constant as temperature increases and, thus, decreases the phonon modes contributing to Eq. (21), and lead to ~50% decrease in the harmonic contributions.[77]

From Eq. (12), the configurational entropy per atom $\Delta S_{\text{conf}}^{\max}$ for a binary is bounded because

$$0 \leqslant \Delta S_{\text{conf}}^{\max} \leqslant -k_B\sum_{n=1}^{2} c_n \ln c_n \leqslant k_B \ln 2. \tag{22}$$

This expression is generalized easily to multicomponent cases, similar to T_c^{est}. Equations (21) and (22) provide an absolute scale to judge the importance of the vibrational effects on T_c. Equally important, $\Delta S_{\text{vibr}}^{\alpha\rightarrow\beta}$ can, in principle, be larger in magnitude than $\Delta S_{\text{conf}}^{\alpha\rightarrow\beta}$ and, moreover, it can be both positive (reducing T_c) or negative (increasing T_c), as evidenced by numerous examples (e.g., see Ref. 8 and references therein).

Here are a few examples for $\Delta S_{\text{vibr}}^{\alpha\rightarrow\beta}$ (in k_B units): From experiment, Delaire, Swan-Wood and Fultz[78] found negative values for V-6.25%Ni, Pd, Pt alloys, from −0.082, −0.185, and −0.272 (all ±0.005), respectively, while for concentrated alloys,[79] Cu_3Au is 0.12±0.03, Fe_3Pt is 0.55±0.03 and $CeSn_3$ is −0.54±0.09. From theory, for example, Cu_3Au is ~0.06.[77] In addition, there are many approximations that have been attempted to reduce the needed phonon calculation,[8] most notably a simple Grüneisen theory.[80] However, these have met with limited success for alloys. For example, some alloys are described by a near-neighbor bond-stretching and bond-bending model,[8] whereas in dilute $Al_{26}Sc$ the vibrational entropy is +0.50 and arise due to longer-ranged

TABLE V. ΔH_{d-o} (in meV), T_c (in K) from Eq. (11), Monte Carlo, and experiment, and percent difference δ (in %) between estimate and Monte Carlo values, for Ca-Sr, Pd-Rh, (Cu,Ag,Au)-Rh, and Au-Pt. $\Delta\chi$ is the difference in the electronegativity of the elements, see text.

	ΔH_{d-o}	T_c^{est}	T_c^{MC}	T_c^{expt}	$T_{\text{melt}}^{\text{expt}}$	δ%	$\Delta\chi$
Ca-Sr							0.05
$Ca_{0.75}Sr_{0.25}$	13.6	280	279		1043	0.4	
$Ca_{0.50}Sr_{0.50}$	17.3	290	290		1011	−0.2	
$Ca_{0.25}Sr_{0.75}$	12.4	256	261		1023	−2.1	
Pd-Rh							0.08
$Pd_{0.75}Rh_{0.25}$	52.0	1074	1091	1033	1913	−1.5	
$Pd_{0.50}Rh_{0.50}$	67.3	1126	1137	1118	2013	−0.9	
$Pd_{0.25}Rh_{0.75}$	49.4	1019	1068	1073	2113	−4.5	
Au-Rh							0.12
$Au_{0.75}Rh_{0.25}$	107.3	2214	2657		1339	−16.7	
$Au_{0.50}Rh_{0.50}$	158.6	2655	2924		1339	−9.2	
$Au_{0.25}Rh_{0.75}$	121.5	2507	2785		1339	−10.0	
Au-Pt							0.20
$Au_{0.75}Pt_{0.25}$	26.1	539	615	1103	1493	−12.4	
$Au_{0.50}Pt_{0.50}$	46.3	776	1021	1513	1573	−24.1	
$Au_{0.4}Pt_{0.6}$	49.2	853	1073	1533	1593	−20.5	
$Au_{0.25}Pt_{0.75}$	45.3	935	1114	1473	1613	−16.1	
Ag-Rh							0.35
$Ag_{0.75}Rh_{0.25}$	148.8	3070	3412		1235	−10.0	
$Ag_{0.50}Rh_{0.50}$	213.2	3570	3586		1235	−0.4	
$Ag_{0.25}Rh_{0.75}$	171.1	3531	3597		1235	−1.9	
Cu-Rh							0.38
$Cu_{0.75}Rh_{0.25}$	31.4	647	882	1103	1533	−26.6	
$Cu_{0.50}Rh_{0.50}$	53.5	896	998	1413	1593	−10.2	
$Cu_{0.4}Rh_{0.6}$	53.4	920	1039	1423	1613	−11.4	
$Cu_{0.25}Rh_{0.75}$	41.9	865	1068	1363	1753	−19.0	

neighbors.[14,81] Note also that for Al-Sc the vibrational entropy is larger than that possible from configurational effects alone. For a more complete picture see the review by van de Walle and Ceder.[8]

Importantly here, however, are recent experimental findings of Delaire and Fultz.[82] For vanadium-based alloys with 6.83%X, where X is taken from 3, 4, and 5d transitional metals, they found that the change in vibrational entropy due to alloying showed a linear correlation with the difference in electronegativity of the constituent elements ($\Delta\chi=\chi_{\text{solute}}-\chi_{\text{host}}$), rather than mass difference, or other possible factors. Essentially, the difference in electronegativity reflects the potential change in local bonding, and, hence, change in bond stiffnesses. The least-squares, linear relation they found was

$$\Delta S_{\text{vibr}}^{\chi} = -0.34\Delta\chi(\pm 0.06\Delta\chi). \tag{23}$$

In addition, reanalysis of their previous results on $L1_2$ metals[47,83] shows that the $\Delta S_{\text{vibr}}^{\chi}$ correlation works,[82] but seems less correct for f electron systems, where even the cluster expansion appears to be more problematic.

Table IV lists the elemental electronegativities χ, and other basic properties, to determine for which systems vibrations might be important. For example, bulk modulus reflects the charge density (hence bonding) at the Wigner-Seitz radius.[85] Let us compare $\Delta S_{\text{vibr}}^{\chi}$ to those already mentioned. For V-Ni and V-Pd, for example, with $\Delta\chi$ of 0.28 and 0.57, $\Delta S_{\text{vibr}}^{\chi}$ is -0.10 ± 0.017 and -0.19 ± 0.034, respectively, in good agreement with experimental values. For Cu_3Au, $\Delta\chi$ is −0.5, so $\Delta S_{\text{vibr}}^{\chi}$ is 0.17 ± 0.03, compared to 0.12 ± 0.03 from above.

Clearly, there is much to be understood in regards to this simple correlation and how it can be used for concentrated alloys, especially its variation with composition and type of order. However, the relevant point is that this approximate correlation permits a quick assessment of when vibrational contributions to T_c can be expected to be important. A synopsis of the transition temperatures for the alloy systems studied are given in Table V, along with ΔH_{d-o} and $\Delta\chi$.

Clearly, from Table V, based upon the correlation with $\Delta\chi$, Ca-Sr and Pd-Rh should have little effect from changes in vibrational modes. Indeed, for Pd-Rh our Monte Carlo and rapid estimate results considering only configurational effects are in good agreement with experiment, as already described. Configurational effects consider only solid-on-solid transformation, which is solid-solution versus segregated state in the present cases. As noted earlier, the stability of the liquid phase is important in the (Ag,Au)-Rh systems, where the predicted T_c exceeds Ag or Au melting temperature T_{melt}.

Importantly, for Cu-rich $Cu_{75}Rh_{25}$ where Rh is solute, $\Delta S_{\text{vibr}}^{\chi}$ is found to be $-0.129k_B$ (using data from Table V), yielding a 30% increase in the configuration-only T_c^{MC} value from (21) at 25% Rh, i.e., from 882 to 1145 K, which is now close to the experimental value of 1103 K, see Table V. Again, how this simple correlation may be used as concentration progresses from 0 to 1, where the "solute" and "host" should change identity, is unclear. Nonetheless the correlation appears to work well, at least within the error in DFT and its vibrational-entropy estimates.

V. CONCLUSIONS

Using first-principles density-functional theory, we calculated the enthalpies of a set of fcc-based phase-segregating alloy systems, found interatomic interactions via the cluster expansion, and determined the transition temperatures (T_c vs c) from Monte Carlo and a rapid mean-field estimate. We predicted that Ca-Sr should segregate at low temperatures, yet to be observed. As validation of our predictions and rapid estimate, we found that Pd-Rh segregates, as is well known, and our T_c results are in excellent agreement with experiment. In addition, we showed that a rapid mean-field estimate of T_c from the ratio of enthalpy and entropy differences between the fully disordered and fully ordered states (obtained analytically within the cluster expansion) agrees well with the Monte Carlo results, permitting rapid design estimates *without* time-consuming Monte Carlo simulations. Using thermodynamic integration, we explained why and when the rapid estimate is accurate and reliable. Finally, we discussed how the difference in constituent electronegativites

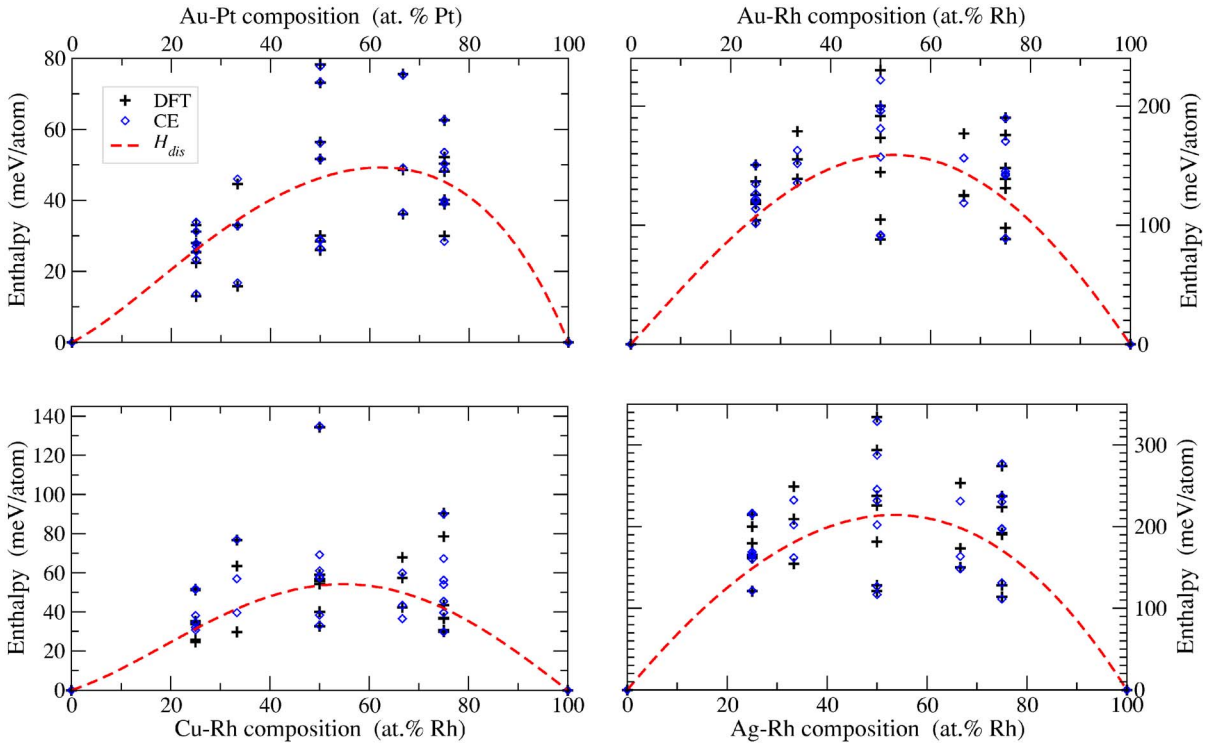

FIG. 5. (Color online) ΔH^F (in meV/atom) versus c for the fcc Au-Pt and Rh-(Au,Ag,Cu) alloys, with symbols as in Fig. 1. Ag-Rh and Au-Rh have 3-4 times larger H_d than Au-Pt or Cu-Rh. Cu-Rh and Au-Pt have similar asymmetry, with the predicted maximum of $H_d(c)$ as observed in T_c vs c, see text. Important influence of liquid phase is discussed in Sec. IV B.

can be used to assess when vibrational entropy should be considered when predicting solid-solid transformations, such as the phase-segregation studied here. For Ca-Sr and Pd-Rh, the configuration-only T_c were shown to be quite good, whereas in Cu-rich Cu-Rh vibrations were estimated to result in a 30% increase in the configuration-only T_c, which then agreed with experiment. How these simple and rapid design-estimate results extend to ordering systems is a part of our ongoing research.

ACKNOWLEDGMENTS

We thank Axel van de Walle for explaining the "smallest-first" algorithm[32] for structure enumeration. We acknowledge financial support in part by NSF Grant No. DMR-0312448 that funds the student development activities, Grant No. DMR-0325939 for critical computer time through the Materials Computation Center, and by DOE Grant Nos. DE-FC36-05GO15064 and DEFG02-03ER46026 for the development of TTK.

APPENDIX: ΔH^F OF Rh-(Cu,Ag,Au) AND Au-Pt

For completeness, we provide the formation enthalpy results in Fig. 5 for various structures at a few concentrations for Au-Pt and Rh-(Cu,Ag,Au) alloys. The similarity to the Ca-Sr and Pd-Rh as far as formation enthalpies are concerned is clear. The numerical results for stoichiometric compositions appear in Table V.

In brief, Au-Pt and Cu-Ru show clear asymmetry in the formation enthalpies, see Fig. 5. For Au- and Ag-Rh systems the formation enthalpies, such as for ΔH_{dis}, are very symmetric. Table I shows the interactions of Au-Pt and Cu-Ru compared to Ca-Sr and Pd-Rh. As expected, due to the asymmetry in the formation enthalpies, there are more significant contributions from multibody interactions. However, more interestingly, the Au-Pt or Cu-Rh pair interactions are of ordering-type, rather than clustering as in Ca-Sr and Pd-Rh. It is the multibodies that are responsible for global clustering, as determined by the sign of the interactions—negative (positive) is clustering (ordering). Ordering or phase segregation are driven by electronic effects,[86,87] especially size effects due to electronic hybridization. Note that the DFT and CE agree very well in Au-Pt system, better than any of the other Rh-(Cu,Ag,Au) systems, showing that the multibodies are critical to reproduce the DFT values. And, as noted in the main text, metastable Au_3Pt has been observed in highly cold-worked Au-rich Au-Pt, and indeed we find that the [100]-layered *A-A-A-B* structure (23 in Sec. II A) has the lowest formation enthalpy (see Fig. 5), in contrast to metastable Au_2Pt structure 9 in Ref. 65.

The simple estimate T_c^{est} can have larger error, see Table V, when the systems exhibit positive curvature in ΔH_{dis}, as happens in both Cu-rich Cu-Rh and Au-rich Au-Pt, which may explain the larger discrepancy between T_c^{est} and T_c^{MC}, as we are investigating. This change in curvature arises from important multibody interactions at dilute concentrations.

*Electronic address: zarkevic@uiuc.edu
†Electronic address: duanej@uiuc.edu

[1] N. A. Zarkevich and D. D. Johnson, Phys. Rev. Lett. **92**, 255702 (2004).
[2] N. A. Zarkevich, Complexity **11**, 36 (2006).
[3] J. W. D. Connolly and A. R. Williams, Phys. Rev. B **27**, R5169 (1983).
[4] J. M. Sanchez, F. Ducastelle, and D. Gratias, Physica A **128**, 334 (1984).
[5] M. Asta, C. Wolverton, D. de Fontaine, and H. Dreyssé, Phys. Rev. B **44**, 4907 (1991).
[6] C. Wolverton, M. Asta, H. Dreyssé, and D. de Fontaine, Phys. Rev. B **44**, 4914 (1991).
[7] J. M. Sanchez, Phys. Rev. B **48**, 14013 (1993).
[8] A. van de Walle and G. Ceder, Rev. Mod. Phys. **74**, 11 (2002).
[9] S. V. Barabash, V. Blum, S. Muller, and A. Zunger, Phys. Rev. B **74**, 035108 (2006).
[10] V. Vaithyanathan, C. Wolverton, and L. Q. Chen, Phys. Rev. Lett. **88**, 125503 (2002).
[11] C. Wolverton and V. Ozoliņš, Phys. Rev. Lett. **86**, 5518 (2001).
[12] N. A. Zarkevich and D. D. Johnson, Phys. Rev. B **67**, 064104 (2003).
[13] N. A. Zarkevich, D. D. Johnson, and A. V. Smirnov, Acta Mater. **50**, 2443 (2002).
[14] V. Ozoliņš and M. Asta, Phys. Rev. Lett. **86**, 448 (2001).
[15] A. Van der Ven, G. Ceder, M. Asta, and P. D. Tepesch, Phys. Rev. B **64**, 184307 (2001).
[16] R. Drautz, H. Reichert, M. Fahnle, H. Dosch, and J. M. Sanchez, Phys. Rev. Lett. **87**, 236102 (2001).
[17] B. D. Krack, V. Ozoliņš, M. Asta, and I. Daruka, Phys. Rev. Lett. **88**, 186101 (2002).
[18] G. L. W. Hart and A. Zunger, Phys. Rev. Lett. **87**, 275508 (2001).
[19] S. Müller and A. Zunger, Phys. Rev. Lett. **87**, 165502 (2001).
[20] N. A. Zarkevich and D. D. Johnson, Surf. Sci. Lett. **591**, L292 (2005).
[21] G. J. Xu, N. A. Zarkevich, Abhishek Agrawal, A. W. Signor, B. R. Trenhaile, D. D. Johnson, and J. H. Weaver, Phys. Rev. B **71**, 115332 (2005).
[22] A. A. Rudnitskiy, R. S. Polyakova, and I. I. Tyurin, Izv. Sekt. Plat. Drug. Blagorodn. Metal. **29**, 190 (1955).
[23] E. Raub, H. Beeskow, and D. Menzel, Z. Metallkd. **50**, 428 (1959).
[24] J. E. Shield and R. K. Williams, Scr. Metall. **21**, 1475 (1987).
[25] *Desk Handbook: Phase Diagrams for Binary Alloys*, edited by H. Okamoto (ASM, Materials Park, Ohio, 2000).
[26] P. E. A. Turchi, G. M. Stocks, W. H. Butler, D. M. Nicholson, and A. Gonis, Phys. Rev. B **37**, 5982 (1988).
[27] D. D. Johnson, P. E. A. Turchi, M. Sluiter, D. M. Nicholson, F. J. Pinski, G. M. Stocks, in *Alloy Phase Stability and Design*, edited by G. M. Stocks, D. P. Pope, and A. F. Gaimei, MRS Symposia Proceedings No. 186 (Materials Research Society, Pittsburgh, 1991), pp. 21–26.
[28] C. Wolverton, D. de Fontaine, H. Dreysse, Phys. Rev. B **48**, 5766 (1993).
[29] Z. W. Lu, B. M. Klein, A. Zunger, J. Phase Equilib. **16**, 36 (1995).
[30] C. B. Alcock and V. P. Itkin, Bull. Alloy Phase Diagrams **7**, 455 (1986).
[31] N. A. Zarkevich, Teck L. Tan, and D. D. Johnson (unpublished).
[32] A. van de Walle (private communications).
[33] L. G. Ferreira, S. H. Wei, and A. Zunger, Int. J. Supercomput. Appl. **5**, 34 (1991).
[34] G. Kresse and J. Furthmüller, Phys. Rev. B **54**, 11 169 (1996).
[35] P. E. Blöchl, Phys. Rev. B **50**, 17953 (1994).
[36] G. Kresse and D. Joubert, Phys. Rev. B **59**, 1758 (1999).
[37] J. P. Perdew, J. A. Chevary, S. H. Vosko, K. A. Jackson, M. R. Pederson, D. J. Singh, and C. Fiolhais, Phys. Rev. B **46**, 6671 (1992).
[38] H. J. Monkhorst and J. D. Pack, Phys. Rev. B **13**, 5188 (1976).
[39] D. D. Johnson, Phys. Rev. B **38**, 12807 (1988).
[40] L. G. Ferreira, A. A. Mbaye, and A. Zunger, Phys. Rev. B **37**, 10547 (1988).
[41] M. E. Arroyo y de Dompablo, C. Marianetti, A. Van der Ven, and G. Ceder, Phys. Rev. B **63**, 144107 (2001).
[42] P. Fratzl and O. Penrose, Acta Metall. Mater. **43**, 2921 (1995).
[43] J.-H. Xu, T. Oguchi, and A. J. Freeman, Phys. Rev. B **35**, 6940 (1987).
[44] P. D. Bogdanoff, B. Fultz, and S. Rosenkranz, Phys. Rev. B **60**, 3976 (1999).
[45] P. D. Bogdanoff, T. L. Swan-Wood, and B. Fultz, Phys. Rev. B **68**, 014301 (2003).
[46] P. D. Bogdanoff, B. Fultz, J. L. Robertson, and L. Crow, Phys. Rev. B **65**, 014303 (2001).
[47] P. D. Bogdanoff and B. Fultz, Philos. Mag. B **81**, 299 (2001).
[48] Z. W. Lu and A. Zunger, Phys. Rev. B **50**, 6626 (1994).
[49] M. Stone, J. R. Stat. Soc. **36**, 111 (1974).
[50] D. Allen, Technometrics **16**, 125 (1974).
[51] K.-C. Li, Ann. Stat. **15**, 958 (1987).
[52] A. van de Walle and G. Ceder, J. Phase Equilib. **23**, 348 (2002).
[53] M. H. F. Sluiter, Y. Watanabe, D. de Fontaine, and Y. Kawazoe, Phys. Rev. B **53**, 6137 (1996).
[54] A. G. Khachaturyan, *Theory of Structural Transformations in Solids* (Wiley, New York, 1983).
[55] H. A. Bethe, Proc. R. Soc. London, Ser. A **150**, 552 (1935).
[56] G. S. Rushbrooke, Proc. R. Soc. London, Ser. A **166**, 296 (1938).
[57] R. Pathria, *Statistical Mechanics* (Pergamon Press, Oxford, 1972).
[58] Sergei Galam, Phys. Rev. B **54**, 15991 (1996).
[59] Sergei Galam, J. Appl. Phys. **87**, 7040 (2000).
[60] N. Metropolis, A. Rosenbluth, M. Rosenbluth, A. M. Teller, and E. Teller, J. Chem. Phys. **21**, 1087 (1953).
[61] A. A. Rudnitskii and A. N. Khotinskaya, Russ. J. Inorg. Chem. **4**, 1160 (1959).
[62] E. Raub, G. Falkenburgh, Z. Metallkd. **55**, 392 (1964).
[63] H. Okamoto and T. B. Massalski, Bull. Alloy Phase Diagrams **5**, 384 (1984).
[64] T. B. Massalski, H. Okamoto, L. Brewer, *Phase Diagrams of Binary Gold Alloys* (ASM International, Metals Park, 1987).
[65] S. Curtarolo, D. Morgan, and G. Ceder, CALPHAD: Comput. Coupling Phase Diagrams Thermochem. **29**, 163 (2005).
[66] F. Doerinckel, Z. Anorg. Chem. **34**, 333 (1907).
[67] C. H. Johnsson and J. O. Linde, Ann. Phys. **5**, 762 (1930).
[68] M. Hansen and K. Anderko, *Constitution of Binary Alloys* (McGraw-Hill, New York, 1958).
[69] H. Okamoto and T. B. Massalski, Bull. Alloy Phase Diagrams **6**, 298 (1985).
[70] A. A. Rudnitskii and A. N. Khotinskaya, Russ. J. Inorg. Chem. **4**, 1053 (1959).
[71] I. Barin, O. Knacke, O. Kubaschewski, *Thermodynamical Properties of Inorganic Substances* (Springer-Verlag, Berlin, 1977).

[72] I. Karakaya and W. T. Thompson, Bull. Alloy Phase Diagrams **7**, 259 (1986).
[73] *CRC Handbook of Chemistry and Physics*, edited by D. R. Lide, (CRC Press, Cleveland, OH, 2003).
[74] M. N. Tamashiro and S. R. Salinas, Phys. Rev. B **56**, 8241 (1997).
[75] F. Ducastelle, *Order and Phase Stability in Alloys* (North-Holland, New York, 1991).
[76] G. D. Garbulsky and G. Ceder, Phys. Rev. B **49**, 6327 (1994).
[77] V. Ozolins, C. Wolverton, and A. Zunger, Phys. Rev. B **58**, R5897 (1998).
[78] O. Delaire, T. Swan-Wood, and B. Fultz, Phys. Rev. Lett. **93**, 185704 (2004).
[79] P. D. Bogdanoff and B. Fultz, Philos. Mag. B **79**, 753 (1999).
[80] V. L. Moruzzi, J. F. Janak, and K. Schwarz, Phys. Rev. B **37**, 790 (1988).
[81] M. Asta and V. Ozoliņš, Phys. Rev. B **64**, 094104 (2001).
[82] O. Delaire and B. Fultz, Phys. Rev. Lett. **97**, 245701 (2006).
[83] P. D. Bogdanoff and B. Fultz, Philos. Mag. B **79**, 753 (1999).
[84] K. A. Gschneider, in *Solid State Physics*, edited by F. Seitz and D. Turnbull (Academic, New Yoirk, New York, 1967), p. 275.
[85] D. Cheng, S. Zhad, S. Wang, and H. Ye, Phys. Rev. B **64**, 024107 (2001).
[86] F. J. Pinski, B. Ginatempo, D. D. Johnson, J. B. Staunton, G. M. Stocks, and B. L. Gyorffy, Phys. Rev. Lett. **66**, 766 (1991).
[87] F. J. Pinski, B. Ginatempo, D. D. Johnson, J. B. Staunton, G. M. Stocks, and B. L. Gyorffy, Phys. Rev. Lett. **68**, 1962 (1992).